ORIGINAL PAPER

Computational assessment of ballistic impact on a high strength structural steel/polyurea composite plate

Tamer El Sayed · Willis Mock Jr · Alejandro Mota · Fernando Fraternali · Michael Ortiz

Abstract Ballistic impact on a polyurea retrofitted high strength structural steel plate is simulated and validated. A soft material model for polyurea, which is capable of capturing complex mechanical behavior characterized by large strains, hysteresis, rate sensitivity, stress softening (*Mullins effect*), and deviatoric and volumetric plasticity, is calibrated against several uniaxial tension experiments and a three-dimensional release wave experiment to capture both the material point and bulk behaviors. A porous plasticity model is employed to model the high strength structural steel and localization elements are included to capture adiabatic shear bands and strain localization. The computational capabilities of these models are demonstrated by the prediction of the target plate displacement, which shows excellent agreement with experiments.

Keywords Ballistic · Polyurea · Projectile · Composite · Viscoelastic · Porous plasticity · Strain localization

T. El Sayed · A. Mota · M. Ortiz (✉)
Division of Engineering and Applied Science,
California Institute of Technology, Pasadena, CA 91125, USA
e-mail: ortiz@aero.caltech.edu

T. El Sayed
e-mail: tamer@caltech.edu

W. Mock Jr
Dahlgren Division, Naval Surface Warfare Center, Dahlgren,
VA 22448-5100, USA

F. Fraternali
Department of Civil Engineering, University of Salerno,
84084 Fisciano (SA), Italy

1 Introduction

Elastomeric polymers have recently been identified as promising for the mitigation of the effects of powerful explosions and the retention of structural fragments that they produce. The polymers can be sprayed or cast on as a lightweight monolithic coating. Different types of reinforcement have been investigated by several researchers. Hybrid light-weight fiber-reinforced polymer–matrix composite laminate armor has been analyzed by Grujicic et al. [5] using a two-dimensional axisymmetric model without fracture. That type of armor is constructed using various combinations and stacking sequences of a high-strength/high-stiffness carbon fiber-reinforced epoxy (CFRE) and a high-ductility/high-toughness Kevlar fiber-reinforced epoxy (KFRE) composite laminates of different thicknesses [5]. Armor consisting of one layer of KFRE and one layer of CFRE, with KFRE laminate constituting its outer surface, possesses the maximum resistance against projectile-induced damage and failure [5].

Laminated composites have shown good potential in reducing armor weight compared to steel for the same ballistic protection, as they result in a 26% weight reduction as compared to steel, according to Ubeyli et al. [15]. Also, the ballistic properties of flax, hemp and jute-fabric reinforced polypropylene composites processed by hot compression moulding were investigated by Wambua et al. [16]. Their ballistic effect was examined by investigating the ballistic limit of composite-steel hybrid systems prepared by gluing thin mild steel plates on the face and rear of the natural fiber composites [16]. Flax composites exhibited better energy absorption than hemp and jute composites and failed by shear cut-out, delamination and fiber fracture [16]. Furthermore, the ballistic properties of the hemp composites increased significantly when a mild steel plate was used as facing and backing [16]. Lin and Fatt [8] have derived analytical

solutions for the deformation, penetration, and perforation of composite plates and sandwich panels subjected to quasi-static punch indentation and projectile impact. A generalized solution methodology for the projectile impact on such structures was developed based on the contact load duration, the through-thickness and the lateral transit times [8]. These methods, however, lack comprehensive contact and fracture models. The ballistic properties of Kevlar 29/Polivnyl Butyral and Polyethylene fiber composites used in the light armor design were analyzed experimentally and numerically by Colakoglu et al. [2]. Higher elastic modulus and strength of Polyethylene composite resulted in a better ballistic performance [2].

In the following sections we describe the finite-element simulation and experimental validation of the ballistic impact of a high speed projectile on a composite plate comprised of high strength structural steel and polyurea. We start in Sect. 2 by describing the constitutive equations used in the material modeling of the metal and polymer. We then proceed in Sect. 3 to outline the fracture model utilized in the validation. In Sect. 4, we detail the equations used in the non-smooth contact approach to model the impact forces. Then, in Sect. 5, we describe the experimental setup and results of the ballistic impact on the metal/polymer composite plate which we validate quantitatively and qualitatively in Sect. 6.

2 Constitutive modeling

2.1 Polymer modeling

A useful characterization of the mechanical behavior of polyurea is supplied by the constitutive model recently proposed in [3,4] for large deformation of soft materials. This model examines the inelastic behavior of such materials, admitting that the mechanical response can be decomposed into equilibrium and non-equilibrium components, representable through an elastoplastic network and several viscoelastic mechanisms (Fig. 1). The elastoplastic component describes long term behavior and permanent material damage, while the viscoelastic components account for time-dependent viscous dissipation.

A variational approach to the constitutive equations (cf. Ortiz and Stainier [12], Yang et al. [19]) is adopted, introducing the following free energy

$$
\begin{aligned}
A^{ep}&(\boldsymbol{F}, \boldsymbol{F}^p, \boldsymbol{Z}^p, T) + A^{ve}(\boldsymbol{F}^p, \boldsymbol{F}_i^v, \boldsymbol{Z}_i^v) \\
&= W^e(\boldsymbol{F}\boldsymbol{F}^{p-1}, T) + W^p(\boldsymbol{Z}^p, T) \\
&\quad + \sum_{i=1}^{M} W_i^e(\boldsymbol{F}\boldsymbol{F}_i^{v-1}, T) + \rho C_v T \left(1 - \log \frac{T}{T_0}\right)
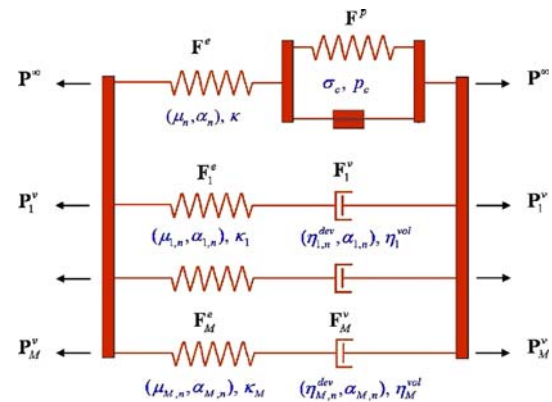\end{aligned}
$$

(2.1)

Fig. 1 Analogy between the proposed constitutive model and a one-dimensional rheological network

where W^e is the elastic strain-energy density associated with the elasto-plastic branch of the developed model; W^p is the plastic stored energy; M is the number of viscoelastic mechanisms; $W_i^e (i = 1, \dots, M)$ are the elastic strain-energy densities corresponding to the viscous relaxation mechanisms (Fig. 1); ρ_0 is the mass density per unit undeformed volume; C_v is the specific heat per unit mass at constant volume and T_0 is the reference temperature. The variables $\boldsymbol{F}^p$, $\boldsymbol{Z}^p$ and $\boldsymbol{F}_i^v$, $\boldsymbol{Z}_i^v$ are related to each other by the means of suitable differential equations *(flow rules)*. The reader should refer to [3,4] for a detailed description of the soft material constitutive model summarized herein.

3 Shear bands

Due to the high strain rate imposed by the ballistic impact, we propose the use of a class of finite elements developed by Yang et al. [18] for capturing sub-grid localization processes such as shear bands and void sheets. The elements take the form of a double surface and deform in accordance with an arbitrary constitutive law. In particular they allow for the development of displacement and velocity jumps across volume element boundaries (Fig. 2).

The thickness of the localized zone is set by an additional field variable which is determined variationally. The localization elements are inserted, and become active, only when localized deformations become energetically favorable. The implementation is three dimensional and allows for finite deformations.

Strain localization are strictly regarded as a *sub-grid* phenomenon and, consequently, the bands of strain localization are modeled as *displacement discontinuities*. These displacement discontinuities are confined to volume-element interfaces and are enabled by the insertion of specialized *strain-localization elements*. These elements consist of two surfaces, attached to the abutting volume elements, which
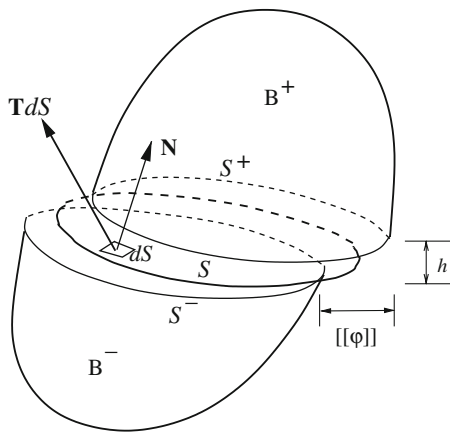
Fig. 2 Localization surface in a three-dimensional body. S^+ and S^- are the *top* and *bottom* (smooth) surface of band attached to the subbody B^+ and B^-, respectively. T is the traction acting on the mid-surface S

can separate and slip relative to each other. The kinematics of the strain-localization elements is identical to the kinematics of cohesive elements proposed by Ortiz and Pandolfi [11] for the simulation of fracture. In contrast to cohesive elements, the behavior of strain-localization elements is governed directly by the same constitutive relation which governs the deformation of the volume elements. As is evident from dimensional considerations alone, the transformation of displacement jumps into a deformation gradient requires the introduction of a length parameter, namely, the band thickness. The band thickness is optimized on the basis of an incremental variational principle [12,19]. This optimization takes the form of a configurational-force equilibrium and results in a well-defined band thickness.

4 Contact potential

A validation of the ballistic impact on a polyurea-reinforced steel plate requires the implementation of a contact potential algorithm capable of recreating the physical contact and frictional forces arising from the impact of the projectile. The contact capability developed by Ortiz and Knap [10] is proposed to model the forces which arise from the impact between the projectile and the target plate. A summary of the contact algorithm follows.

Let the kinetic energy of the body be given by

$$T(\dot{\varphi}) = \int_{B_0} \frac{1}{2} \rho_0 \dot{\varphi} \cdot \dot{\varphi} \, dV_0, \qquad (4.1)$$

in which φ is the position, dV_0 is a material or referential differential of volume, and ρ_0 is the mass density in the reference configuration.

The potential energy of the body has contributions from the strain energy of the bulk material, the applied load, the body forces, and an indicator function that plays the role of the contact potential, as follows

$$V(\varphi) = \int_{B_0} w(F) \, dV_0 - \int_{B_0} \rho_0 b \cdot \varphi \, dV_0$$
$$+ \int_{\partial_t B_0} [I_C(\varphi) - t \cdot \varphi] \, dS_0 \qquad (4.2)$$

in which φ is the position, F is the deformation gradient, $w(F)$ is the stored energy function for the bulk material, dV_0 is a material or referential differential of volume, b is the body force density per unit mass, $\partial_t B_0$ is the part of ∂B_0 in which the boundary traction t is specified, and $I_C(\varphi)$ is an indicator function defined as

$$I_C(\varphi) = \begin{cases} 0, & \text{if } \varphi \in C, \\ \infty, & \text{otherwise,} \end{cases} \qquad (4.3)$$

in which C is the set of admissible configurations φ in which interpenetration does not occur [6].

The Lagrangian function for the body is then

$$L(\varphi, \dot{\varphi}) = T(\dot{\varphi}) - V(\varphi), \qquad (4.4)$$

which gives rise to the action integral

$$I[\varphi] := \int_0^T L(\varphi, \dot{\varphi}) \, dt, \qquad (4.5)$$

which, according to Hamilton's variational principle, yields the equation of motion for the system when extremized.

The action integral (4.5) reaches an extremum when its variation with respect to its independent variables is zero, as follows

$$\delta I = \int_0^T \left(\int_{B_0} (\rho_0 b \cdot \delta\varphi - P : \delta F - \rho_0 \ddot{\varphi} \cdot \delta\varphi) \, dV_0 \right.$$
$$\left. + \int_{\partial_t B_0} (t - F^{\text{con}}) \cdot \delta\varphi \, dS_0 \right) dt$$

$$= \int_0^T \left(\int_{B_0} (\nabla \cdot P^T + \rho_0 b - \rho_0 \ddot{\varphi}) \cdot \delta\varphi \, dV_0 \right.$$
$$\left. + \int_{\partial_t B_0} (t - F^{\text{con}} - P \cdot N) \cdot \delta\varphi \, dS_0 \right) dt$$

$$= 0$$

in which $F^{con} := \partial I_C(\varphi)/\partial \varphi$ are the contact forces. The Euler–Lagrange equation corresponding to (4.5) is then

$$\nabla \cdot P^T + \rho_0 b = \rho_0 \ddot{\varphi} \quad \text{on } B_0,$$
$$P \cdot N + F^{con} = t \quad \text{on } \partial_t B_0,$$
$$t = 0 \quad \text{on } S_0. \tag{4.6}$$

The admissible configurations in which interpenetration does not occur are such that

$$\varphi \in C \iff g_\alpha(\varphi) \geq 0, \quad \alpha = 1, \dots, N_p \tag{4.7}$$

in which $g_\alpha(\varphi)$ are constraints that prevent penetration, and N_p is the number of such constraints. One choice for the constraint functions is the interpenetrating distances between the surface defined by the contact potential and the target. In this way N_p becomes the number of interpenetrating distances. The indicator function can then be approximated as

$$I_C(\varphi) \approx k \sum_{\alpha=1}^{N_p} g_\alpha^3(\varphi), \tag{4.8}$$

in which k is a penalty parameter.
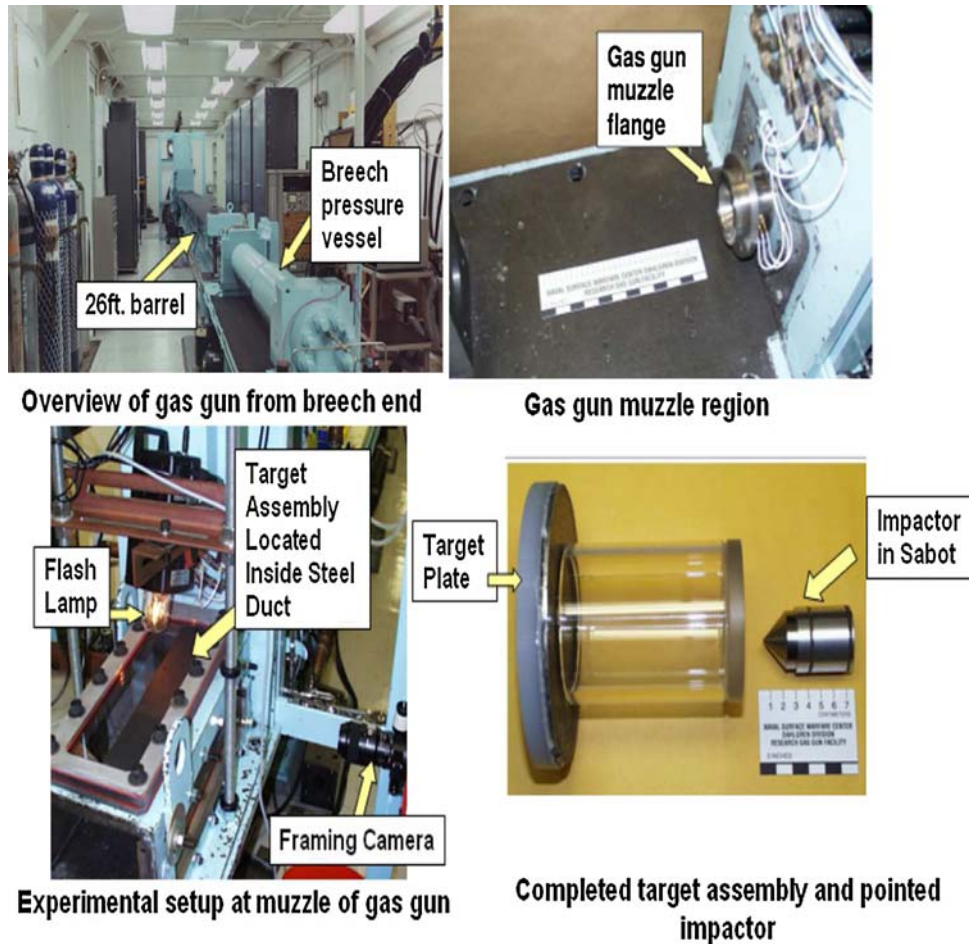
5 Impact experiment

The impact experiment to be validated was performed by Mock et al. [9] at the Research Gas Gun Facility at the Naval Surface Warfare Center (Dahlgren Division) (see Fig. 3). A 4340 steel impactor is launched as shown in Fig. 4 at a composite circular plate comprising high strength structural steel and cast on polyurea (see Table 1 for short details). The impactor strikes the target plate on the steel side at a speed of 280.9 m/s causing it to deform significantly along with the polyurea coating. Displacement profiles are recorded at various times and compared to the validation simulation.

6 Validation

6.1 Polyurea tension tests

The experimental data considered for polyurea under tension was provided by [14]. The reported results were obtained on a newly developed drop-weight tensile test instrument that ensures strain rate uniformity and strain homogeneity. Shuttle speeds as high as 26 m s^{-1} were achievable, corresponding

Fig. 3 Naval Surface Warfare Center (Dahlgren Division) Research Gas Gun Facility and target assembly
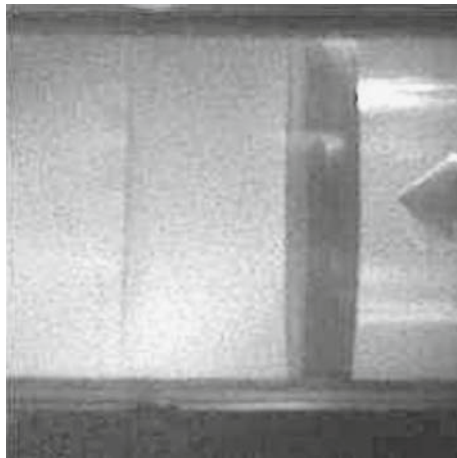
**Fig. 4** Impactor (*right*) about to strike target composite plate (*left*)

Table 1 Impact experiment parameters

Impactor mass (g)	145
Impactor hardness (RC)	36
High strength structural steel target plate mass (g)	692.2
High strength structural steel target plate diameter (mm)	154.2
High strength structural steel target plate average thickness (mm)	4.75
Polymer mass (g)	230.1
Polymer diameter (mm)	154.2
Polymer thickness (mm)	11.1
Polymer/steel thickness ratio	2.335
Impact speed (m/s)	280.9

to strain rates $\sim 10^3$ s^{-1} [14]. Tests were conducted at strain rates varying from 0.15 s^{-1} (quasi-static) to 408–573 s^{-1} (high strain rates). The initial region is linear, with a slope

approaching 100 MPa at the highest rates. There is also an increase in stiffness as the strain rate increases (see Fig. 5). Considering all of these factors, Genetic Algorithms (GAs) were utilized to determine sets of parameters for the experiments. It is important to note that the Ogden parameters thus obtained are stiffer as the strain rate increases (see Table 2).

Fig. 5 Tension tests on polyurea. Cauchy stress versus true strain (all corrected for inertial forces), with the corresponding strain rates as indicated. The model Cauchy stresses are also shown for the same strain rates. The experimental curves were obtained from [14]
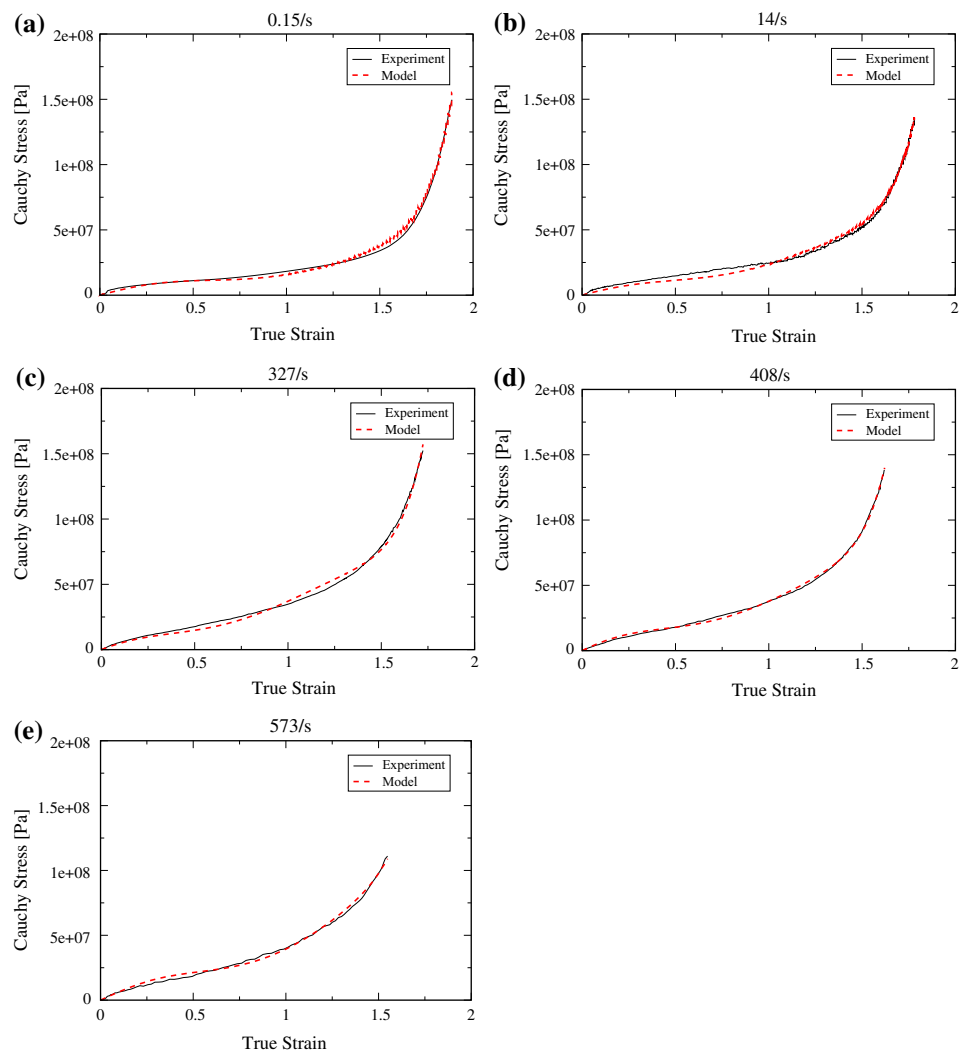
Table 2 Model parameter estimates for tension tests on polyurea at various strain rates

Strain rate (s^{-1})	0.15	14	327	408	573
μ_1 (Pa)	34.45	55.0	96.92	154.26	148.64
α_1	7.44	7.44	7.5	7.29	7.84
μ_2 (Pa)	33.67	51.8	100 .78	146.93	154.15
α_2	7.86	7.47	7.46	8.01	6.09
μ_3 (Pa)	32.72	53.62	98.6	153.57	147.87
α_3	5.33	7.64	7.58	6.65	5.03
τ_1 (s)	2.02	0.0195	0.0006	0.0005	0.0005
$\mu_{1,1}$ (Pa)	1.73×10^6	1.83×10^6	2.79×10^6	2.68×10^6	2.55×10^6
$\alpha_{1,1}$	4.72	4.0	4.0	6.0	5.58
$\mu_{1,2}$ (Pa)	1.6×10^6	1.84×10^6	2.44×10^6	2.54×10^6	2.59×10^6
$\alpha_{1,2}$	4.5	4.28	4.11	4.58	5.39
$\mu_{1,3}$ (Pa)	1.97×10^6	1.92×10^6	2.79×10^6	252×10^6	2.46×10^6
$\alpha_{1,3}$	4.78	4.21	4.29	6.0	5.47
τ_2 (s)	41.66	0.355	0.0116	0.00992	0.00992
$\mu_{2,1}$ (Pa)	192218	483001	937288	942297	718477
$\alpha_{2,1}$	4.62	4.47	4.5 8	4.46	4.44
σ_0 (Pa)	5.59×10^6	6.57×10^6	5.64×10^6	6.47×10^6	5.59×10^6
ϵ_0^p	1.1	1.1	1.1	1.01	1.1
n	0.005	0.005	0.005	0.004	0.001

Also, in agreement with [14], viscoelastic behavior is evident, with the result that the mechanical properties of polyurea in tension are highly rate-dependent (Table 2). The model is evidently able to capture these complex behaviors via three Ogden terms in deviatoric elasticity, two relaxation mechanisms (the first with three Ogden terms and the second with only one), and deviatoric plasticity.

6.2 Polyurea bulk behavior

The material parameters of polyurea obtained in Sect. 6.1 are at a material point, therefore the polyurea bulk behavior needs to be identified before the impact experiment can be validated. For this particular impact experiment, the polyurea approximately elongates to a strain of 0.104 (by observing the displacement results) during the first 270 μs after the impactor strikes the target, resulting in a strain rate of 380 s^{-1}. The 408 s^{-1} strain rate material parameters obtained in Sect. 6.1 were used in a three-dimensional finite element simulation of a release wave experiment (see Fig. 6) conducted by Clifton [1] at Brown University with an impact velocity of 218.2 m/s.

The existence of voids in polyurea was observed in the microstructure of the spall area (Fig. 7) which called for the activation of volumetric plasticity in the model. Contact was also utilized in order to capture the effect of the reflected wave
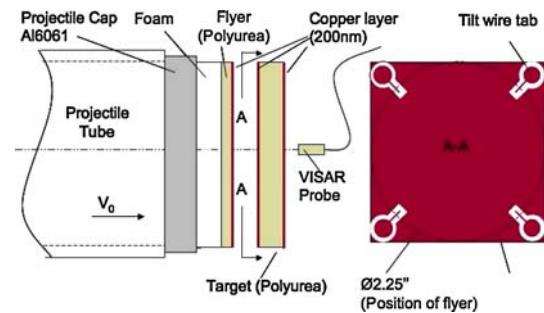
Fig. 6 Polyurea release wave experimental setup by Clifton et al. [1]
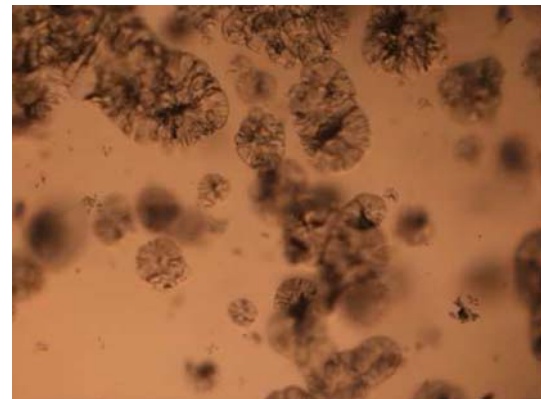
Fig. 7 Microstructure of the damaged area in polyurea as a result of the release wave experiment [1]
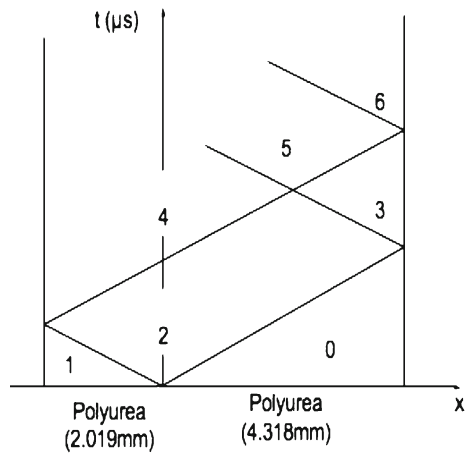
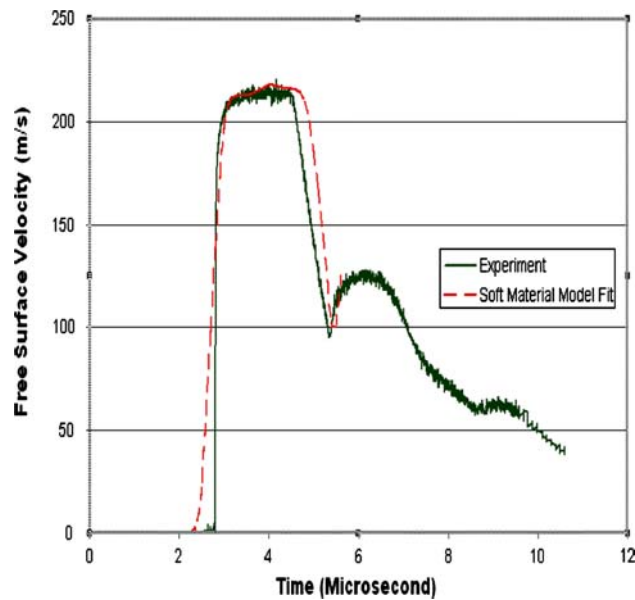**Fig. 8** $T - x$ diagram of the release wave experiment [1]

Fig. 9 Free surface normal velocity versus time. Experimental curve was obtained from [1]

in the flyer as it passes through the interface and reaches the original wave in the target plate resulting in spall, as shown in Fig. 8. The second peak in Fig. 9 is caused by the reflected wave from the spall plain reaching the free surface. Spall was captured in the validation via insertion of localization elements, however, the experiment was fitted only up to the end of the first peak in order to capture the wave speed (bulk behavior) in the material, which was the intended objective of this calibration.

The simulated normal velocity of the target free surface is shown to be in good agreement with the experimental results (see Fig. 9). The bulk parameters obtained for this validation are shown in Table 3. It is important to note that cyclic tests, which include tension and compression, are needed in order to obtain a more comprehensive set of parameters.

**Table 3** Material parameter estimates for release wave experiment on polyurea [1]

ρ (kg/m^3)	1070
ν	0.495
Void radius a_0 (m)	81.6×10^{-7}
Void density N_v (voids/m^3)	2.89×10^{12}
μ_1 (Pa)	150
α_1	7.5
μ_2 (Pa)	150
α_2	7.5
μ_3 (Pa)	150
α_3	7.5
τ_1 deviatoric (s)	4.90×10^{-4}
τ_1 volumetric (s)	4.90×10^{-4}
$\mu_{1,1}$ (Pa)	2.6×10^6
$\alpha_{1,1}$	5.0
$\mu_{1,2}$ (Pa)	2.6×10^6
$\alpha_{1,2}$	5.0
$\mu_{1,3}$ (Pa)	2.6×10^6
$\alpha_{1,3}$	5.0
τ_2 deviatoric (s)	9.94×10^{-3}
τ_2 volumetric (s)	9.94×10^{-3}
$\mu_{2,1}$ (Pa)	0.95×10^6
$\alpha_{2,1}$	4.5
σ_0 (Pa)	6.0×10^6
ϵ_0^p	1.0
n	0.003

Table 4 Porous plasticity model material parameter estimates for high strength structural steel

ρ (kg/m^3)	7700
E (GPa)	210.0
ν	0.29
σ_0 (Pa)	400.0×10^6
ϵ_0^p	0.004
n	6.0
$\dot{\epsilon}_0^p$ (s^{-1})	0.001
m	60.0
T_0 (K)	293
T_m (K)	1371
C_v (J kg^{-1} K^{-1})	486.0
α (K^{-1})	12.0×10^{-6}
l	0.75
β	0.9
Void radius a_0 (m)	5.2×10^{-9}
Void density N_v (voids/m^3)	1.0×10^{22}

Table 5 Thermal parameter estimates for polyurea

|	
T_0 (K)	293
T_m (K)	500.0
C_v (J kg^{-1} K^{-1})	1.5×10^3
α (K^{-1})	4.0×10^{-5}
l	1.0
β	0.5
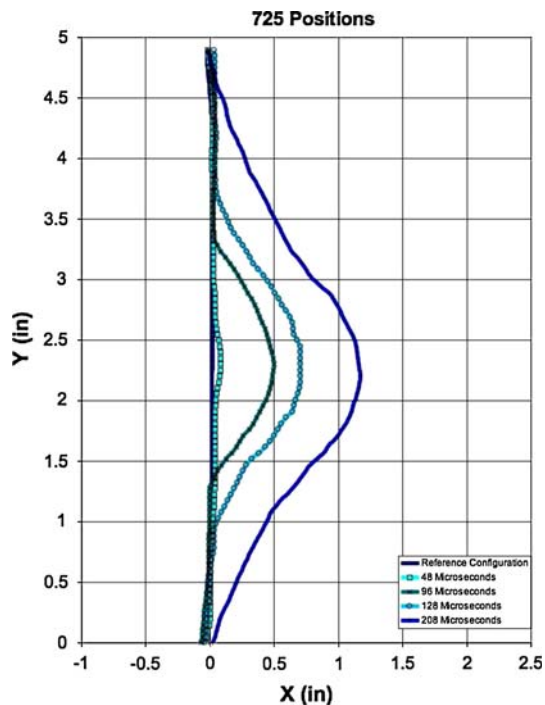
Fig. 10 Measured composite plate positions at different times after impact. Each symbol represents a time frame. Refer to the web version of this article for colored representation of the time frames

6.3 Discussion

A mesh comprising 25605 fully-integrated 10-noded composite tetrahedral elements was constructed in adherence to the dimensions outlined in Table 1. Delamination was not observed in the experiment, hence, the nodes were joined at the interface between the high strength structural steel and polyurea to model the cast on condition without delamination. The model outlined in this work was utilized for polyurea with the activation of thermal softening allowing for the formation of shear bands (thermal properties obtained from Katti et al. [7] and Primeaux Associates LLC are shown in Table 5). The parameters obtained for polyurea in Sects. 6.1 and 6.2 were assigned to the polyurea elements. A porous plasticity model outlined by Weinberg et al. [17] was utilized for the high strength structural steel yielding the material properties shown in Table 4. Friction was modeled as in Reid and Hiser [13] with values of 0.15 and 0.1 for the static and
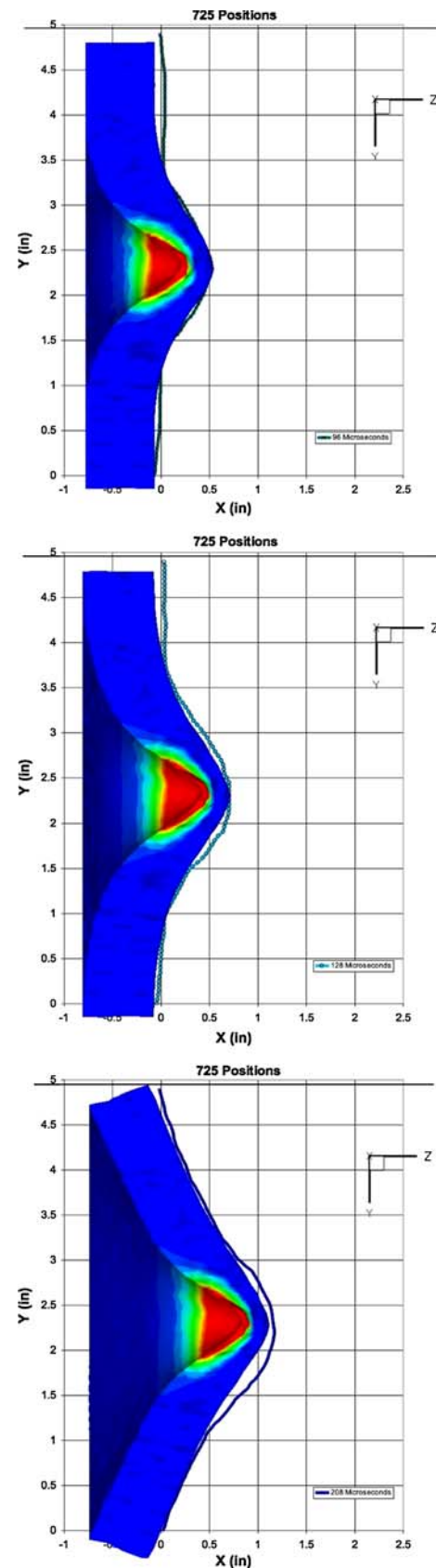
**Fig. 11** Experimental and computational displacements at various times after impact
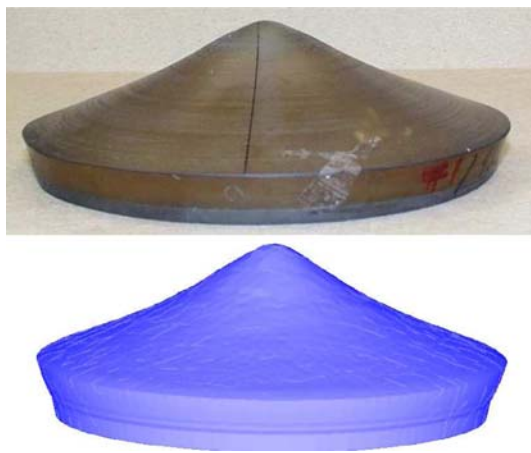
Fig. 12 Experimental (*top*) and computational (*bottom*) final configurations. The computational configuration is at 208 μs after impact

kinetic friction coefficients, respectively. The experimental displacement profiles were recorded at various times after the composite plate was impacted for the purpose of validation (see Fig. 10). The simulation was performed on 256, 2.4 GHz, Intel Xeon processors with 4 GB of memory shared between every 2 processors. The calculation lasted for approximately 72 h to reach 297 μs. It is observed in the experiment that the composite target plate starts to move as a rigid body along with the impactor at approximately 200 μs after impact. The simulation displacement profiles were consequently compared to the experimental results up to 208 μs after impact with very good agreement, as shown in Fig. 11. Localization elements, right after insertion, capture shear bands without fracture. As the deformation within the shear band increases, the stress decreases due to softening in the material as the deformation becomes exceedingly large. When the stress becomes zero, then one can consider that the localization element is inactive and in effect a free surface exists, i.e., a crack, which did not occur in the experiment, nor in the simulation. The final configurations at 208 μs after impact are shown in Fig. 12 and contours of the plastic strain, volumetric strain, and temperature are shown in Figs. 13 and 14.

7 Conclusions

A ballistic impact on a polyurea-retrofitted composite plate is simulated and validated and the computational capability for assessing such impacts is established. A constitutive model which combines finite viscoelasticity, finite elastoplasticity, and decoupling of volumetric and deviatoric responses is utilized to model the polyurea response. A future area of research would be to use computer simulations to model failure at the interface; an important objective would be to use the simulations to isolate signatures for a specific failure mode.
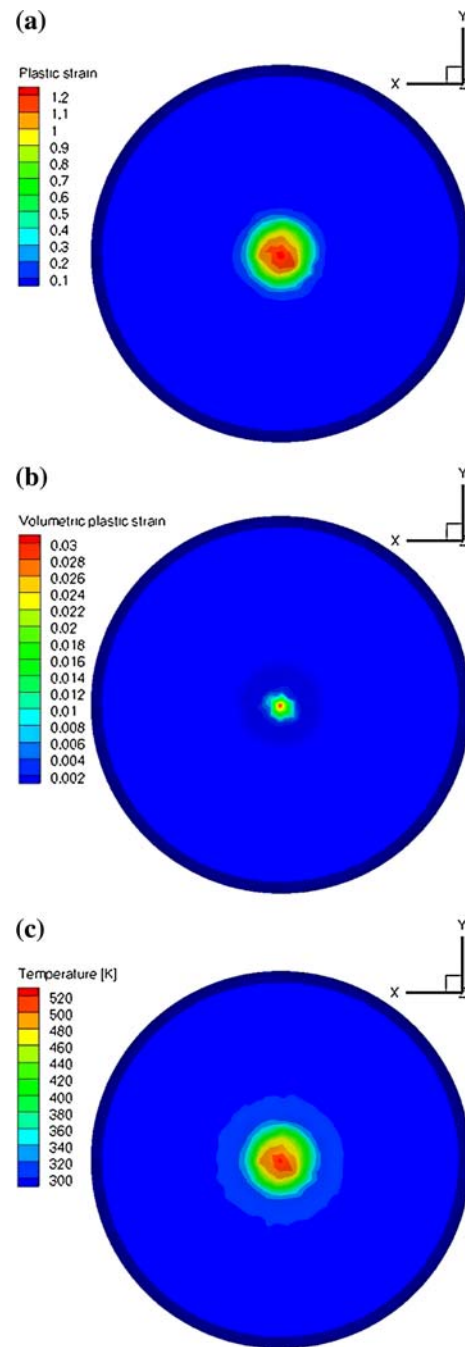
Fig. 13 Plastic strain (**a**), volumetric strain (**b**), and temperature (**c**) contour plots from the impact side of the composite plate at 208 μs after impact

Moreover, future work will include extending the adopted model to include viscoelastic cavitation effects, accounting for the coupling between void growth and deviatoric deformation, thermal conductivity, heat capacity and conversion of dissipated work into heat.

Applications of the present material and ballistic modeling include optimal design and assessment of a variety of structures under dynamic loading, and the optimization of
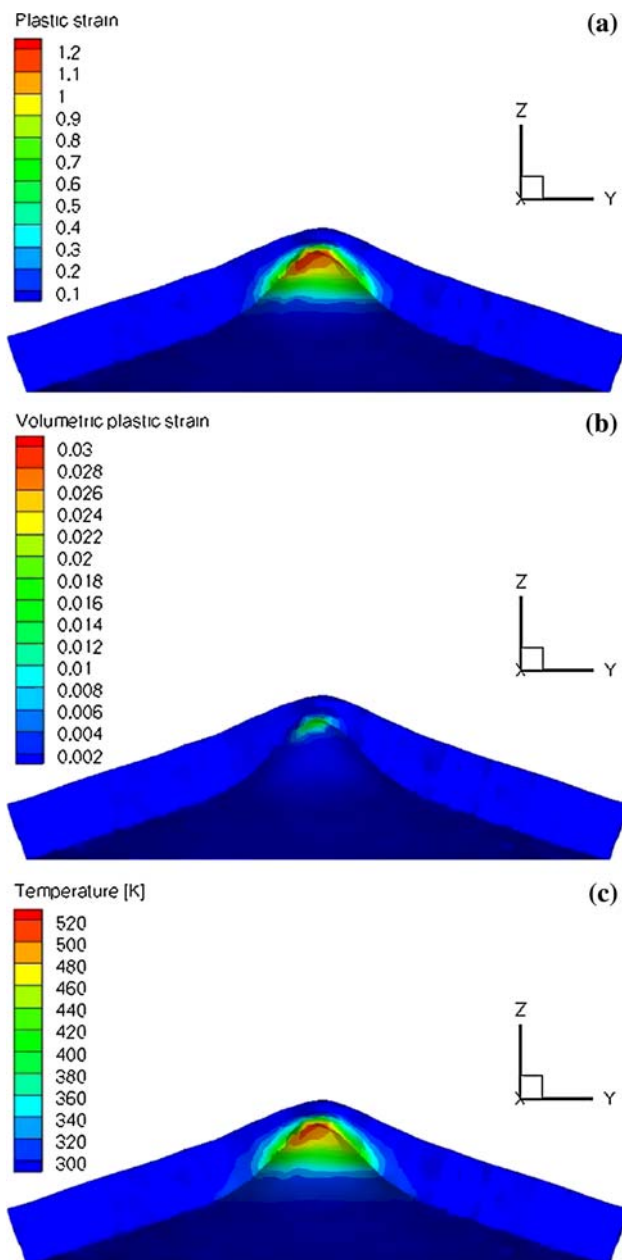
Fig. 14 Plastic strain (**a**), volumetric strain (**b**), and temperature (**c**) contour plots across the thickness of the composite plate at 208 μs after impact

crash and impact performance of polymer retrofitted structures, with special attention to polymer-steel sandwich plates, honeycomb composites, polymers or foam padding and multi-layered coatings. These studies would be particularly helpful in designing high-strength composites and the next-generation of armors that can better withstand ballistic impact.

References

1. Clifton RJ (presenter), Jiao T, Grunschel S (2006) Deformation and failure of an elastomer at very high strain rates. 15th U.S. National Conference on Theoretical and Applied Mechanics
2. Colakoglu M, Soykasap O, Özek T (2007) Experimental and numerical investigations on the ballistic performance of polymer matrix composites used in armor design. Appl Compos Mater 14:47–58
3. El Sayed T (2007) Constitutive models for polymers and soft biological tissues. PhD thesis, California Institute of Technology
4. El Sayed T, Mota A, Fraternali F, Ortiz M (2008) A variational constitutive model for soft biological tissues. J Biomech 41(7): 1458–1466
5. Grujicic M, Pandurangan B, Koudela KL, Cheeseman BA (2006) A computational analysis of the ballistic performance of light-weight hybrid composite armors. Appl Surf Sci 253:730–745
6. Kane C, Repetto EA, Ortiz M, Marsden JE (1999) Finite element analysis of nonsmooth contact. Comput Method Appl M 180(1–2): 1–26
7. Katti A, Shimpi N, Roy S, Lu H, Fabrizio EF, Dass A, Capadona Lynn A, Leventis N (2006) Chemical, physical, and mechanical characterization of isocyanate cross-linked amine-modified silica aerogels. Chem Mater 18:285–296
8. Lin C, Fatt M (2006) Perforation of composite plates and sandwich panels under quasi-static and projectile loading. Compos Mater 40:1801–1840
9. Mock W Jr (presenter), Drotar J (2006) Penetration protection experiments using polymer materials. ONR Workshop, St. Michael's, Maryland
10. Ortiz M, Knap J (2003) Effect of indenter-radius on au(001) nanoindentation. Phys. Rev. Lett. 90(22)
11. Ortiz M, Pandolfi A (1999) Finite-deformation irreversible cohesive elements for three-dimensional crack-propagation analysis. Int J Numer Methods Eng 44(9):1267–1282
12. Ortiz M, Stainier L (1999) The variational formulation of viscoplastic constitutive updates. Comput Method Appl M 171(3-4): 419–444
13. Reid JD, Hiser NR (2004) Friction modeling between solid elements. I J Crash 9(1):65–72
14. Roland CM, Twigg JN, Vu Y, Mott PH (2007) High strain rate mechanical behavior of polyurea. Polymer 48(2):574–578
15. Übeyli M, Yıldırım RO, Ögel B (2007) On the comparison of the ballistic performance of steel and laminated composite armors. J Mater Des 28:1257–1262
16. Wambua P, Vangrimde B, Lomov S, Ignaas V (2007) The response of natural fibre composites to ballistic impact by fragment simulating projectiles. Compos Struct 77:232–240
17. Weinberg K, Mota A, Ortiz M (2006) A variational constitutive model porous metal plasticity. Comput Mech 37:142–152
18. Yang Q, Mota A, Ortiz M (2004) A class of variational strain-localization finite elements. Int J Numer Methods Eng 62(8): 1013–1037
19. Yang Q, Stainer L, Ortiz M (2006) A variational formulation of the coupled thermo-mechanical boundary-value problem for general dissipative solids. J Mech Phys Solids 54:401–424